ELSEVIER

Physica B 314 (2002) 386–390

PHYSICA B

www.elsevier.com/locate/physb

Monte Carlo particle-based simulation of FIBMOS: impact of strong quantum confinement on device performance

I. Knezevic*, D. Vasileska, R. Akis, J. Kang, X. He, D.K. Schroder

Department of Electrical Engineering and Center for Solid State Electronics Research, Arizona State University, Tempe, AZ 85287-5706, USA

Abstract

A 250 nm focused-ion-beam MOSFET (FIBMOS) has been simulated using a two-dimensional coupled Monte Carlo–Poisson particle-based solver, in which quantum effects have been taken into account by incorporating an effective potential scheme into a classical particle simulator. Inclusion of quantum effects in the analysis of FIBMOS operation is crucial because the high doping density of the p^+-implant leads to strong quantum confinement of carriers at the implant/oxide interface. We show that the device drive current, threshold voltage and transconductance are indeed extremely sensitive to the proper treatment of quantization.

Keywords: FIBMOS; Quantum effects; Monte Carlo simulation; Device modeling

1. Introduction

In the design of ultra-small devices, one has to deal with two conflicting requirements: (1) diminishing of short-channel effects, which necessitates the use of high substrate doping densities, and (2) hot-carrier reliability improvement and substrate current reduction, both requiring lower in-plane electric field and, therefore, lower substrate doping density. Extensive theoretical and experimental effort to optimize semiconductor devices in compliance with the above requirements has resulted in structures such as the lightly doped drain (LDD) devices, gate overlapped LDD structure (GOLD), halo source GOLD drain (HS-GOLD) [1], graded-channel MOS (GCMOS) [2], and focused-ion-beam MOSFET (FIBMOS) [3]. FIBMOS device structure is characterized by a focused-ion-beam (FIB) p^+-implant near the source end of the channel (see Fig. 1). Benefits of the FIBMOS device with respect to a conventional MOSFET have been analyzed through hydrodynamic [3–5] and Monte Carlo simulations [5–8].

In this paper, we present a particle-based Monte Carlo–Poisson simulation of a 250 nm FIBMOS, with the inclusion of quantum effects through an *effective potential* [9]. Incorporation of quantum effects into the simulation of a FIBMOS device is crucial because the FIB implant high doping density leads to strong quantum confinement of carriers at the implant/oxide interface. We will begin by discussing the use of the effective potential and the rationale behind it. The simulation results and the device output characteristics will then be presented, and the impact of quantum effects on the device performance will be discussed.

*Corresponding author. Fax: +1-480-965-8058.
E-mail address: irenak@asu.edu (I. Knezevic).

0921-4526/02/$ - see front matter
PII: S0921-4526(01)01427-2

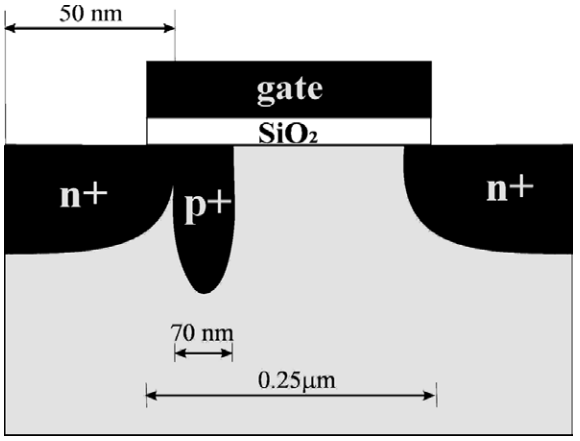

Fig. 1. A schematic picture of the simulated 250 nm FIBMOS device.

2. Effective potential

The inclusion of one-particle quantum effects in the description of inversion at the semiconductor/oxide interface of a metal-oxide–semiconductor device involves solving the Schrödinger equation for the carriers in an approximately triangular potential well. As a result, one obtains bound states, which give rise to two major features: *reduced sheet density* and *charge set-back*. Namely, since the lowest bound state can be regarded as the new bottom of the conduction band, the spacing between the Fermi level and the conduction band edge is effectively increased, which results in the reduced sheet charge density with respect to the case in which quantum effects are excluded. Moreover, the probability density in the lowest bound state now has a maximum away from the semiconductor/oxide interface, resulting in charge displacement from the oxide, which accounts for an effective increase in the oxide thickness.

The so-called *effective potential* [9] offers a simple and rather effective approximate treatment of quantum effects. It naturally takes into account the spreading of an electron wave packet in a quantized system, thereby mimicking the solution of the Schrödinger equation, while, on the other hand, it is easily incorporated into classical particle simulators. The effective potential, V_{eff}, is related to the self-consistent Hartree potential, V, obtained from the Poisson equation, through an integral smoothing relation

$$V_{\text{eff}}(\boldsymbol{x}) = \int V(\boldsymbol{x}+\boldsymbol{y})G(\boldsymbol{y},\boldsymbol{a}_0)\,\mathrm{d}y, \tag{1}$$

where G is a Gaussian with the standard deviation $\boldsymbol{a}_0$. V_{eff} is then used to calculate the electric field that accelerates the carriers in the transport kernel of the simulator. The use of V_{eff} has a fairly low computational cost ($<10\%$ increase in CPU time), but it creates instabilities in the Monte Carlo–Poisson solver, thus increasing the time needed to arrive at steady-state conditions.

The actual value of the smoothing parameter a_0 and its dependence on the potential profile are obvious issues when implementing this approach [10]. Here, it suffices to say that the use of a single smoothing parameter, $a_0 = 0.64\,\text{nm}$, throughout the active region of the device, is proven to quite accurately describe the quantum effects that originate from the spreading of the carrier wave-packet.

3. Results and discussion

The simulated 250 nm FIBMOS device is shown schematically in Fig. 1. The substrate doping density equals $10^{16}\,\text{cm}^{-3}$, the oxide thickness is 5 nm, the width of the FIB region is 70 nm, and the

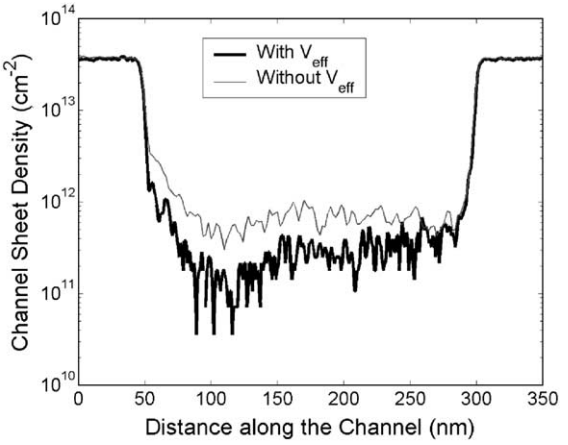

Fig. 2. Sheet carrier density for $V_{\text{D}} = V_{\text{G}} = 1.0\,\text{V}$, with and without V_{eff}.

implant doping is $1.6 \times 10^{18}\,\mathrm{cm}^{-3}$. Since the substrate doping density is fairly low, the quantum effects are negligible in most of the channel, but are extremely important at the immediate p^+-implant/oxide interface, where the channel is narrowest.

As discussed in the previous section, there is an upward shift of the conduction band edge near the semiconductor–oxide interface when V_{eff} is included to account for the quantum effects. Consequently, the carrier sheet density is lower with V_{eff} than without it, as shown in Fig. 2 for the gate voltage (V_{G}) and drain voltage (V_{D}) both equal to 1 V. (In Figs. 2–4 the distance along the channel is measured from the device boundary at source end; source/drain width is 50 nm.) Moreover, the sheet density, both with and without V_{eff}, has a minimum in the p^+-implant part of the channel, where inversion is most difficult to achieve.

In Figs. 3a and b the electron density near the source end of the channel is shown. Near the source (i.e. at the implant/oxide interface) the channel is wider with V_{eff} (Fig. 3a) than without it (Fig. 3b). This charge set-back leads to an additional capacitance in series with the oxide capacitance, which results in the device transconductance degradation.

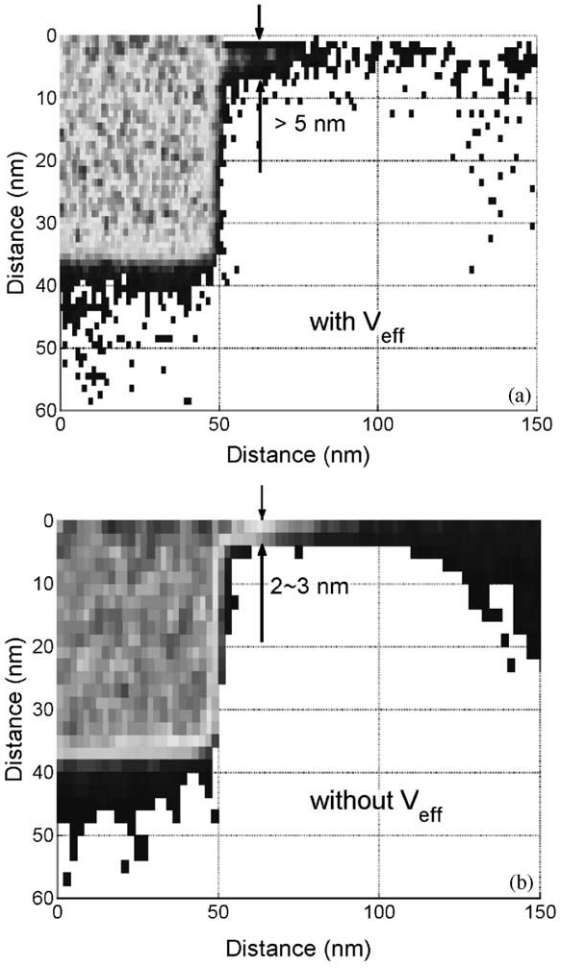

Fig. 3. Electron density near the source end of the channel, for $V_{\mathrm{D}} = V_{\mathrm{G}} = 1.0$ V: (a) with V_{eff} and (b) without V_{eff}.

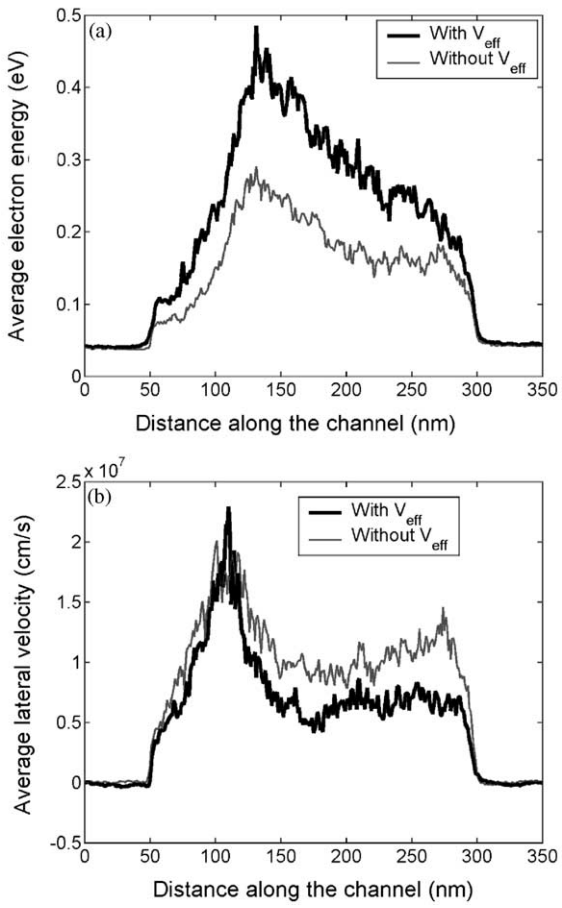

Fig. 4. (a) Average carrier energy and (b) average lateral velocity of carriers along the channel, for $V_{\mathrm{D}} = V_{\mathrm{G}} = 1.0$ V.

The behavior of the average carrier energy along the channel is presented in Fig. 4a, whereas Fig. 4b shows the lateral velocity profile. The average carrier energy (Fig. 4a) increases if V_{eff} is included because the 'new' bottom of the conduction band is higher in energy than the 'old' one, which is the zero kinetic energy level. Higher average energy also means that scattering is facilitated, and consequently mobility is degraded [10] and the average velocity is lowered, as seen in Fig. 4b. The obtained behavior of the average energy and average velocity when V_{eff} is included agree with the corresponding features reported for a conventional MOSFET [11].

In Fig. 5 the current–voltage characteristics of the FIBMOS device for V_{G} equal to 1.0 and 1.2 V, with and without V_{eff}, are presented. There are three noteworthy features in Fig. 5: with V_{eff}, the drive current is reduced, the threshold voltage (V_{th}) is increased, and the transconductance is degraded. The inclusion of V_{eff} reduces the drain current I_{D}, due to both the reduced average carrier velocity and the reduced sheet density, the latter being predominant. Also, since the slope of the $I_{\mathrm{D}}-V_{\mathrm{D}}$ curve in the linear region is proportional to $V_{\mathrm{G}}-V_{\mathrm{th}}$, we see that for a given V_{G} the inclusion of V_{eff} increases V_{th}, in agreement with the reduction in sheet density, as presented in Fig. 2. And finally, if for a given V_{D}, we analyze the current increase between V_{G} equal to 1.0 and 1.2 V, which is (roughly) proportional to transconductance, it is clear that the transconductance is lower with V_{eff} included, as expected according to the charge set-back depicted in Figs. 3a and b.

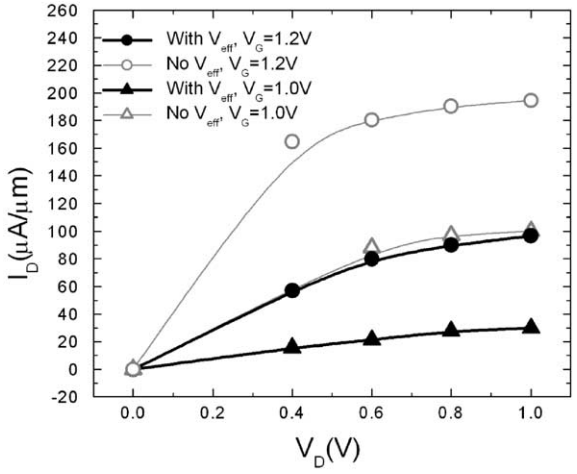

Fig. 5. Current–voltage characteristic of the simulated FIBMOS device, with and without V_{eff}, for $V_{\mathrm{G}}=1.0$ and 1.2 V.

4. Conclusion

We employed an effective potential approach to account for the quantum-mechanical effects in a 250 nm FIBMOS device. The inclusion of quantum effects leads to a reduced sheet density and the set-back of the channel carriers from the semiconductor/oxide interface, which are manifested in the significantly reduced drive current, increased threshold voltage and degraded transconductance. The obtained features are evidence that treatment of quantum-mechanical effects becomes crucial when estimating the performance of asymmetrically doped devices, in which the very narrow and very deep confining potentials, present in the highly doped regions, give rise to prominent quantum-mechanical behavior of carriers.

Acknowledgements

The authors would like to thank Massimo M. Fischetti and Steven M. Goodnick for valuable discussions during the preparation of this manuscript. The financial support from SRC, the Office of Naval Research under Contract No. N000149910318 and the National Science Foundation under NSF-CAREER ECS-9875051 are also acknowledged.

References

[1] T.N. Buti, et al., IEEE Trans. Electron. Devices 38 (1991) 1757.
[2] J. Ma, et al., IEEE Trans. VLSI Syst. 5 (1997) 352.
[3] C.C. Shen, et al., IEEE Trans. Electron. Devices 45 (1998) 453.

[4] J. Kang, D.K. Schroder, in: Technical Proceedings of the Third International Conference on Modeling and Simulation of Microsystems, San Diego, California, March 27–29, 2000, p. 356.
[5] M. Stockinger, et al., Microelectron. J. 30 (1999) 229.
[6] A. Hiroki, et al., IEDM Tech. Dig. (1995) 439.
[7] S. Odanaka, A. Hiroki, IEEE Trans. Electron. Devices 44 (1997) 595.
[8] J. Kang, et al., VLSI Design, in press.
[9] D.K. Ferry, Superlattices Microstruct. 27 (2000) 61.
[10] I. Knezevic, et al., submitted for publication.
[11] D.K. Ferry, et al., IEDM Tech. Dig. (2000) 287.